The 7th KAI Aerospace Thesis Prize

Development of Micro Aerial Vehicle Systems and Autonomous Formation Flight of Multi-MAVs

Advisor: Professor Shim, Hyunchul

(hcshim@fdcl.kaist.ac.kr, 042-350-3724)

by

You, Dong Il

(diyou@fdcl.kaist.ac.kr, 042-350-3764)

School of Mechanical, Aerospace and Systems Engineering,

Division of Aerospace Engineering

KAIST

Development of Micro Aerial Vehicle Systems and Autonomous Formation Flight of Multi-MAVs

Abstract

The objective of this paper is to design and develop autonomous micro aerial vehicle (MAV) systems. A specific mission profile is proposed for design requirement of vehicle and autopilot system. The aircraft design is carried out by conventional design procedures. Thin airfoil theory is applied to analyze and develop vehicle airfoil. An In-house CATIA – MATLAB code is developed for airfoil analysis. The power system is chosen by using a thrust calculator with various motors, propellers and batteries. The MAV's linear SISO longitudinal dynamics and lateral dynamics are obtained using MATLAB Identification Toolbox for controller design. The autopilot controller for autonomous navigation flight consists of attitude, altitude hold and waypoint navigation guidance loop. The multi-loop classical controller is implemented for attitude control in inner loop. The controller is designed based on that identification results. Then, a high speed flight computer is developed to operate multi-flight processes such as navigation, GPS, communication process and so on. An autopilot is integrated by combinations of GPS, IMU, flight computer and PWM board. It is applicable to advanced control techniques due to its high speed and powerful performance. The autonomous waypoint flight result with this system shows good performance and is turned out to be robust under cross wind condition. Finally, the control law for formation flight is designed via 'leader - follower' formation method using active link for inter-communication.

1. Introduction

During the past two decades, unmanned aerial vehicles (UAV) have been developed for military and commercial purposes. After war in Afghanistan and Iraq where the UAVs are launched an offensive, UAVs have shown its capabilities for various applications due to its outstanding mission achievements. With the interest of UAV is rapidly growing up, the micro aerial vehicles (MAVs) have been brought out for its portability and low operation cost while it has excellence reconnaissance capability and low visual observability.

According to the US Unmanned Roadmap 2032, The Defense Advanced Research Projects Agency **(**DARPA**)** and the US Army are focused on a small UAV system suitable for backpack deployment and single-man operation. Each military personnel will carry an MAV and portable computer for reconnaissance and detection of chemical air pollution in the future war field [1].

Following with these military visions, the MAV Researches are transforming man oriented mission achievement to fully autonomous and intelligent mission operation recently. In additions, it is required that small UAVs and MAVs which are equipped with low-cost sensors and computers operate and perform the missions simultaneously to get information of targets effectively in surveillance area.

Black widow was the first successful MAV with automatic control system providing altitude, heading and airspeed hold without GPS sensor [2]. The Brigham Young University developed the autonomous vehicle with 8bit 29MHz micro-computer. The vehicle had a 60.5cm wingspan. The University of Florida MAV team has developed an autonomous MAV having a maximum linear dimension of 31cm. It is equipped with autopilot, GPS, modem and so on. And also, the University of Arizona developed MAV which can fly autonomously [2].

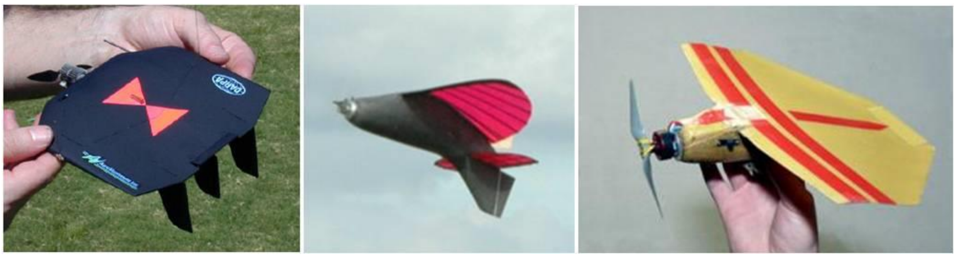

Fig. 1 Black Widow (Left), UF MAV (Middle) and Arizona MAV (Right)

Although these vehicles can perform automatic flight, they are not capable of high level control such as formation flight, task allocations for cooperation with other MAVs because of autopilot performance. Hence, the high performance of autopilot is required to apply modern control techniques and various capabilities for multi-MAVs operation in practical such as dynamic path planning, formation flight and collision avoidance.

Formation flight control is an essential technique for multi-UAVs or MAVs with high performance autopilot. Generally, formation flight of bird species has been performed to take advantage of the aerodynamic benefits. The traditional 'V' formation flown by birds not only helped communication between individuals, but also decreased the induced drag for each trailing bird, and it lead to reducing the energy for flying [2].

Fig. 2 Formation Flight of Birds

For UAV applications, formation flight can raise the operational capability of UAVs and increases its chances of success during carrying out their missions. Moreover, since the MAV has a constraint on payload and flight time, formation flight of MAV makes the MAVs allocate its tasks with each other.

Therefore, the objective of this research is to design a specialized aircraft which is matched mission profile considering low Reynolds aerodynamics and develop powerful autopilot system. And also, linear SISO models are determined to design the MAV controller. In additions, autonomous formation flight control law is proposed for maximizing MAV operational capabilities.

2. Aircraft Design

The MAV design process that consists of conceptual design, preliminary design, manufacturing and flight test is the same as conventional aircraft development. It is shown below in Fig. 3.

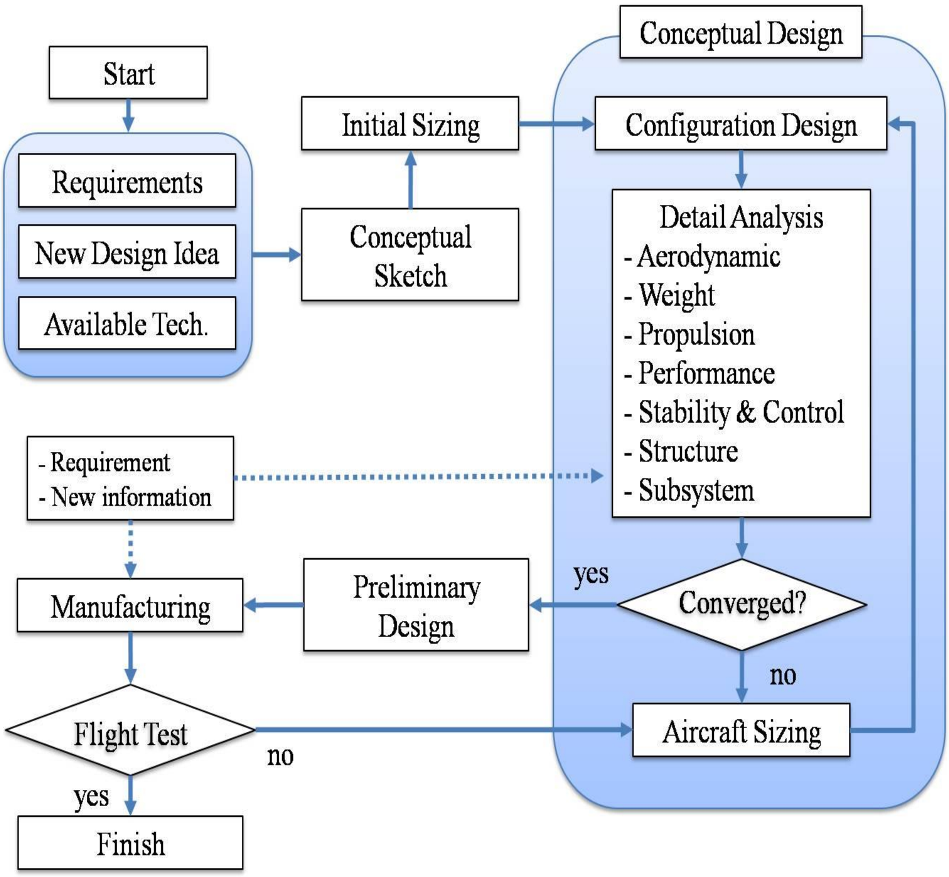

Fig. 3 MAV Design Process

In regard of the steps of MAV design, each design stage is described in next in more detail.

2.1 Conceptual Design

In this section, the MAV mission profile, design requirements, and estimation of thrust - weight ratio (T/W) and wing loading (W/S) are considered and described as a conceptual design phase. Considerations of configuration are introduced to set an outline for preliminary design step.

First of all, the mission profile of MAV is designed as shown in Fig. 4.

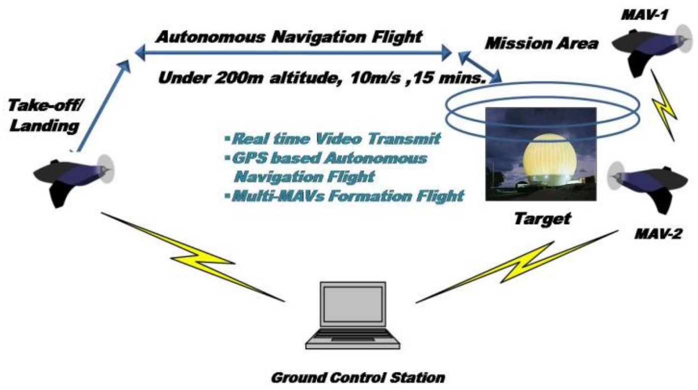

Fig. 4 MAV Mission Profile

The mission profile is one of the most significant parts of aircraft design, because it directly relates to an aircraft requirement of performances such as weight and endurance of vehicle. During operation of the whole missions, the aircraft carries out the mission with autopilot system which provides fully autonomous navigation and formation flight to cooperate with other vehicles. The required aircraft performances are set as 10 m/s of cruising velocity and 15 minutes of operational flight time under 200 meter altitude. As can be seen in Fig. 4, the MAVs are controlled by Ground Control Station (GCS). They collaborate with each other and transmit data to GCS at mission area.

Second, the design requirement of MAV is set as shown in Table.1 based on the mission profile given above.

Table. 1 Design requirement

Max. Size	500 mm
Max. Weight	400 g
Cruise Velocity	10 m/s
Cruise Altitude	100 m
Min. Endurance	15 min
Payload	150 g

The payload is set as 150g in result of weight estimation of the autopilot system which is described in section 4. From Table. 1, the maximum empty weight of MAV is under 250g to meet the design requirements.

The next step is estimation of required thrust and wing area for initial sizing of MAV. Typically thrust - weight ratio (T/W) and wing loading (W/S) are used to design. The thrust - weight ratio (T/W) and wing loading (W/S) are the two most important parameters affecting aircraft performance. The thrust - weight ratio (T/W) means the ratio of take-off weight to maximum throttle level thrust at sea level static, standard day condition. And wing loading (W/S) is the ratio of design gross weight to the reference wing area. In design phase, one of the parameters should be guessed and it is used to calculate the other parameter from the critical design requirements.

The T/W of MAVs has usually 0.6 ~ 0.7 which is little higher value as compared with conventional aircraft's T/W except for jet fighters as shown in Table. 1. The T/W for the MAV is set as 0.7 based on that.

Table. 1 Thrust to Weight ratio (T/W) [3]

Aircraft Type	Typical installed T/W
Univ. Florida MAV	0.6
Spyplanes's MAV	0.7
Jet trainer	0.4
Military Cargo/bomber	0.25
Jet Transport	0.2 ~ 0.4

Then, the required T_{max} is calculated at about 2.75 N with T/W ratio of 0.7. It means that the propulsion system have to provide more than 2.75 N. This is considered as a baseline to select power system in section 2.2.3.

Table. 2 Wing loading (W/S) [4]

Aircraft	W/S (kg/m^2)
Black Widow - Generation 1	2.7
INHA univ. - AR-722	4.0
Konkuk univ. - Batwing	4.0
Univ. of Florida MAV	3.0 ~ 5.0 (estimation)
Sailplane	30
Homebuilt	54

Usually, the MAVs have the low wing loading as represented in Table. 2. W/S of MAV is set as 2.5, because the W/S ratio is dependent on component weight which is getting lighter and smaller recently.

Then, the required reference wing area is calculated at 0.16 m^2 and it is used as a main design parameter in wing design.

In order to maximize MAV's capabilities and aerodynamic performances, it is necessary to consider some design parameters and limiting factors for conceptual sketch such as drag, weight and maximum size of vehicle.

The MAV is preferred to be a tailless type aircraft in order to minimize drag and weight which are essential for better performance. A reflexed airfoil has to be adopted for longitudinal stability of tailless type aircraft. At the same time, the MAV should have an elevator for pitch control and a rudder for roll and yaw control without horizontal tail.

On the other hand, some design parameters, for example, aspect-ratio and wing area, should be maximized for the performances. The wing area has to be designed by using calculated wing reference area before.

2.2 Preliminary Design

2.2.1 Airfoil Design and Analysis

The MAV development begins with airfoil design to get desired aerodynamic performance such as C_l, C_m. The traditional aircraft have Reynolds number in range 10^6 and are designed to achieve laminar flow over most of the airfoil. However, the laminar separation bubble is major concern of aerodynamic performance. It is formed when laminar flow over an airfoil encounters an adverse pressure gradient large enough that the laminar flow lacks the flow momentum to overcome the gradient and separates [5]. The Fig. 5 represents details of the laminar separation bubble forming. The laminar separation bubble makes an increase in drag and a reduction of lift [6].

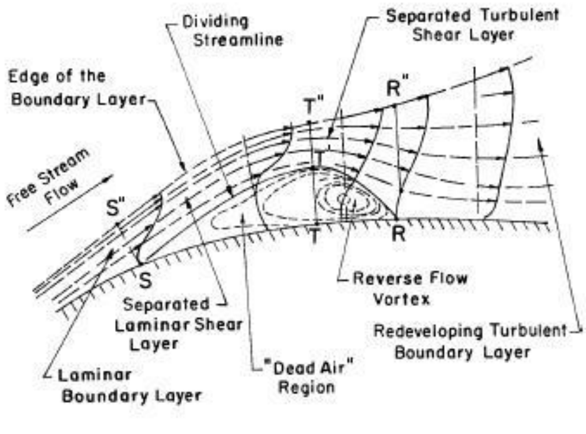

Fig. 5 Laminar Separation Bubble [6]

To avoid these disadvantages on aerodynamic performance a thin-cambered airfoil is usually selected and it also takes an advantage of weight reduction. In terms of stability, the airfoil is required to be reflexed, since the MAV is designed to be tailless [7]. With all of these considerations most of the airfoil design approaches define the airfoil as an n^{th} order polynomial mean camber line. This approach is easy to analyze the aerodynamic characteristics of the airfoil such as C_l, C_m using Thin Airfoil Theory (THT) [8, 9]. The airfoil is approximated as an 8^{th} order polynomial equation to analyze as shown in Eq.(2.1). The MAV's airfoil design is conducted with iterative modifications of airfoil through THT analysis result and a series of flight test. For these design procedure in-house CATIA - MATLAB code is developed to analyze airfoil characteristics directly when the airfoil is designed.

The developed airfoil is designed with 5.5% camber at 20% of chord and 2.5% reflex camber at 90% of chord. The Fig. 6 and Table. 4 show the geometry of airfoil and aerodynamic analysis result using THT.

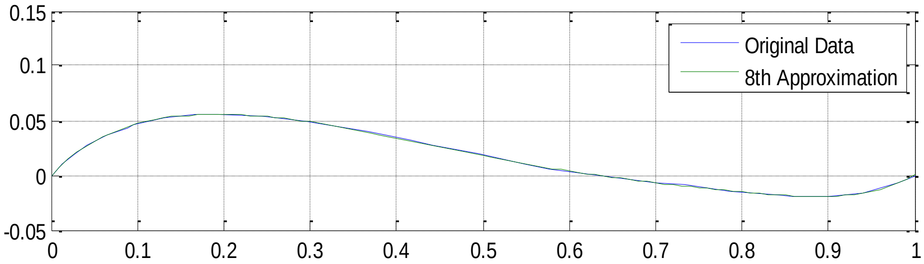

Fig. 6 Designed 8^{th} reflex airfoil geometry

$$z = a_1\left(\frac{x}{c}\right)^8 + a_2\left(\frac{x}{c}\right)^7 + \ldots + a_8\left(\frac{x}{c}\right) + a_9 \tag{2.1}$$

$$a = [-4.6650 \quad 28.6096 \quad -63.8082 \quad 71.6925 \ldots$$
$$-46.1083 \quad 18.6493 \quad -5.2169 \quad 0.8483 \quad -0.0002]$$

Table. 3 Reflex airfoil data

Max. Chord	Max. Camber	Max. Camber position	Reverse Camber	Reverse Camber position
393mm	5.5%c	20%c	2.5%c	90%c

* 'c' means chord of airfoil.

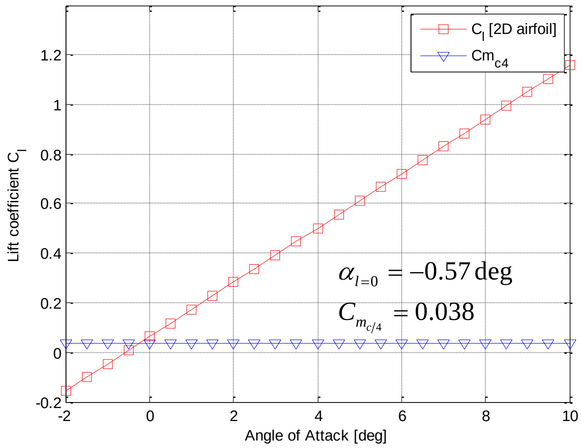

Fig. 7 THT analysis result of reflex airfoil

2.2.2 Wing and Airframe Design

There are some design parameters to consider when developing a wing including gross take-off weight, wing shape, maximum span location, aspect ratio etc. There are additional constraints that have to be maximized for aerodynamics properties. The maximizing parameters are wing area for ensuring enough lift and design requirement, aspect ratio for minimizing induced drag, and maximum span location for minimizing wingtip vortex affecting wing surface flow [10]. Therefore, the wing shape is based on inverse Zimmerman type wing. The design is based around thorough utilization of a sphere, where diameter is the chosen maximum length 500mm of aircraft. These considerations and constraints are converted into geometric drawing and the revised inverse Zimmerman wing for the MAV is developed as shown in Fig. 8.

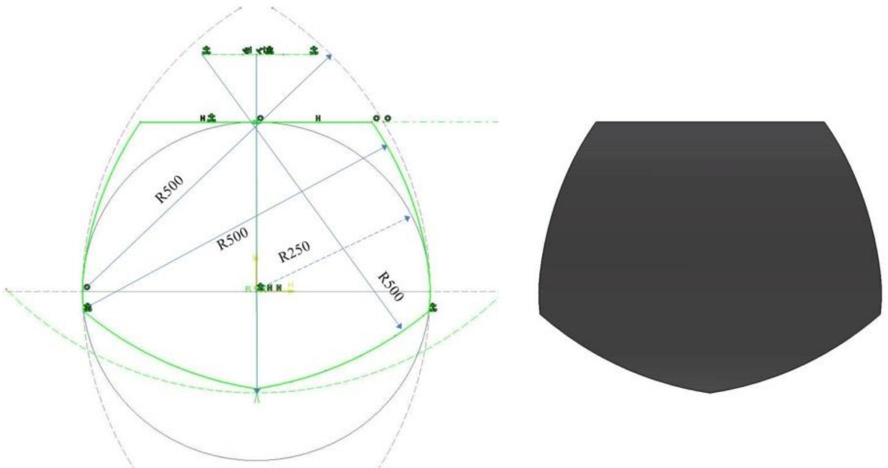

Fig. 8 Wing geometric sketch and Shape

Table. 5 Wing geometric data

Mean Aerodynamic Chord(MAC)	Reference Wing area	Aspect ratio	Max Span location
393mm	0.163m^2	1.53	0.7 c

The wing geometric data is represented in Table. 5. From now on, the C_{Lreq} and can be calculated using wing area and other values. The flight condition of MAV is assumed that it is in steady level flight condition at 10m/s and 50m height.

$$
\begin{aligned}
L &= \frac{1}{2}\rho V^2 S\, C_{L_{wing}} = W \\
C_{L_{req}} &= \frac{2W}{\rho V^2 S} = 0.393
\end{aligned}
\tag{2.2}
$$

The next step is fuselage design based on an outline made in conceptual sketch. The goal for the airframe is to focus on securing static stability of MAV. For longitudinal stability, it is necessary for the wing to have reflex and for center of gravity (CG) to be located forward in direction of X axis. To be stable in lateral axis the aircraft should have a high - wing configuration with low CG point in direction of Z axis. Finally, to guarantee stability in directional axis the fuselage must have the shape of symmetric airfoil and streamlined body and vertical tail. On the basis of these outlines, the airframe of MAV is developed using CATIA. The Fig. 9 shows the picture of MAV.

In addition, static margin is one of important parameter for stability. A conventionally balanced aircraft is usually designed to have positive static margin in range of 0.03 to 0.05. It is defined as Eq. (2.3).

$$SM = \frac{x_{AC} - x_{CG}}{MAC} = -\frac{dC_M}{dC_L} \quad [14] \tag{2.3}$$

The aerodynamic center of an airfoil tends to locate at 0.25 c in subsonic speed. Therefore, X_{AC} is 89mm and the X_{CG} is 65mm which is obtained by flight test. Then, the static margin (SM) of MAV is calculated as 0.067. It ensures that the MAV is stable longitudinally.

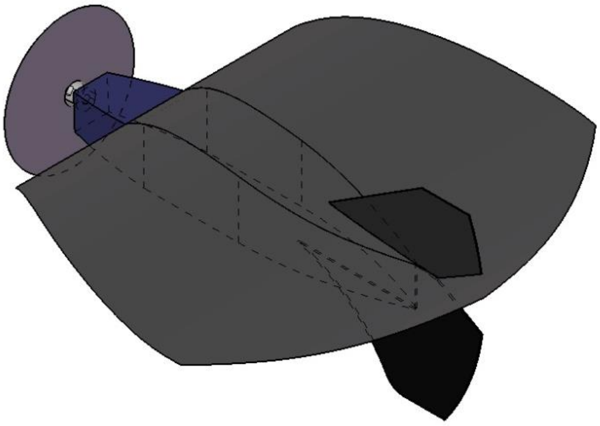

Fig. 9 3D view of KAIST MAV

2.2.3 Power System

The power system consists of a brushless motor and Li-polymer battery. Required T_{max} of MAV is already calculated in conceptual design by using T/W ratio. And the C_{D0} of MAV is estimated at 0.05 that is bigger than the model aircraft of C_{D0} in range of 0.018 to 0.031 [11]. Using and the same flight conditions in Section 2.2.2, the required thrust for level flight can be obtained as follows.

$$\begin{aligned} C_D &= C_{D_0} + \frac{C_{L_{level}}{}^2}{\pi AR\, \mathrm{e}} \\ D &= \frac{1}{2}\rho V^2 S\, C_D = T \\ T_{req_{\,level}} &= 1.11N,\; T_{\max} \geq 2.75N \end{aligned} \tag{2.4}$$

The motor is selected in consideration of available T_{max} and having a light weight. It is operating based on 2cell Li-polymer battery as power source. The selected motor can produce maximum static thrust of 3.73N consuming 11.6A with a 6x4 propeller The required thrust for level flight is set as 1.5N to get design margin to make up for uncertainties of estimated parameters such as C_{D0} and cruising velocity and so on. As you can see in Fig 10, the required power is 15W for level flight. It is increased in 24.2W due to 62% of driving efficiency. Using Fig.10 the required current can be estimated at 5.5A for level flight. This is essential for the calculating of required battery capacity with desired endurance. It can be obtained as follows.

$$Duration[\min] = \frac{60 \times Capacity[mAh]}{Current[A] \times 1000}\,[12] \tag{2.5}$$

The calculated capacity of battery should be more than 1375mAh. The autopilot system which is described in detail later consumes 0.5A for operation. The required capacity for the autopilot system is estimated at 250mAh with 30 minutes for operating. Total capacity of battery is 1625mAh. Based on this estimation, the battery is chosen appropriately.

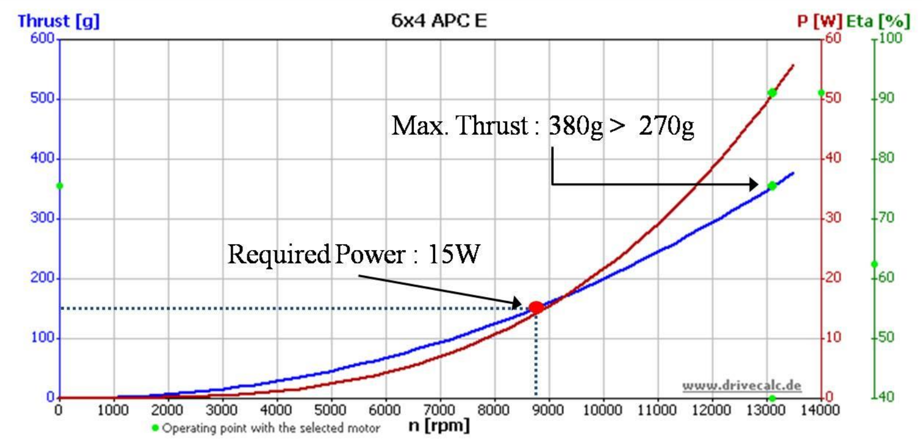

Fig.10 Thrust vs RPM vs Power Chart [13]

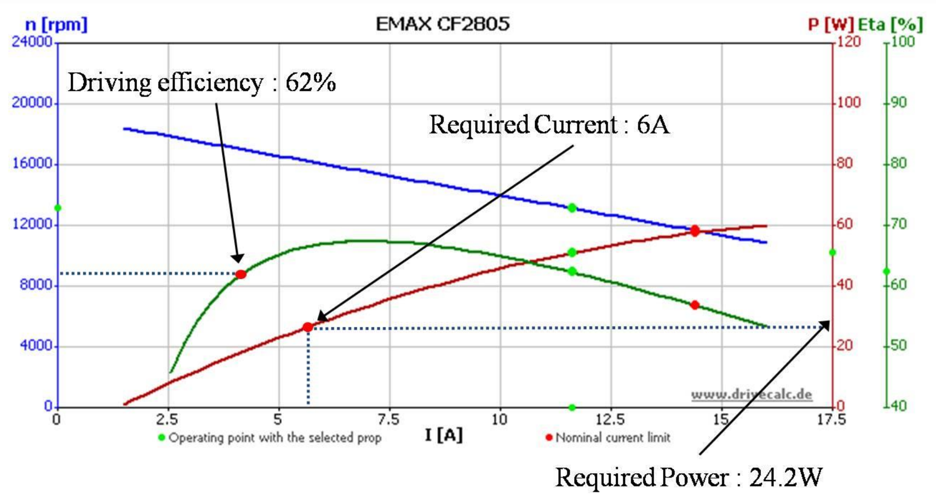

Fig.11 Thrust vs Current vs Power Chart [13]

2.3 Construction and Flight Test

The main objectives for construction are that materials must be durable, light weight and easy to get. As mentioned before in section 2.1, the maximum empty weight is set as 250g and the weight restriction for airframe can be obtained by using components weight estimation. Table. 6 provides a component list and associated weights.

Table. 4 Component breakdown

Component		Weight (g)	
Propulsion System	Motor	30	125
	Battery	80	
	ESC	15	
RC System	Receiver	15	35
	Servos	20	
Autopilot System (payload)	Computer	25	95
	GPS	20	
	IMU	20	
	PWM board	15	
	Misc. (connectors and wire)	15	
Total		255	

The airframe should have light weight within about 150g to meet a design outline. With weight constraint and desired material property for construction, it is not so many types of materials around. After measuring weight and testing manufacturability of various kinds of materials such as carbon, fiber glass, balsa, EPP and foam board, the foam board combined with EPP and PVC is chosen for reason of consideration of construction objectives. Fig.12 presents the complete configuration of MAV.

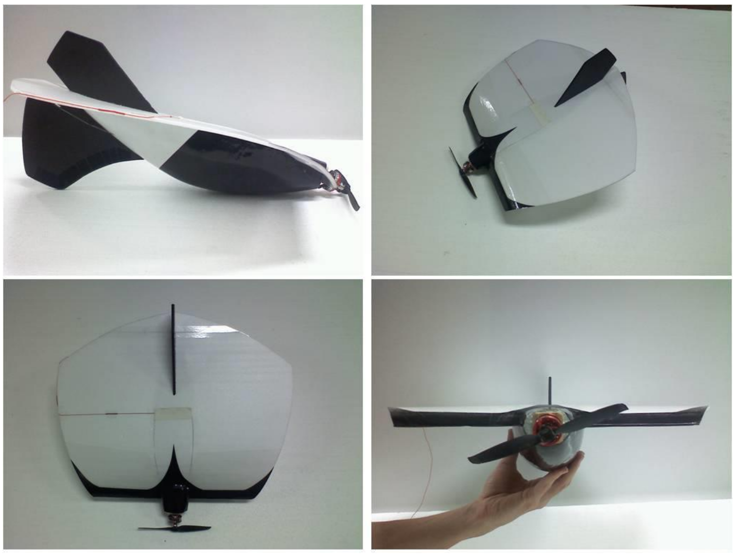

Fig.12 MAV configurations

The airframe has 90g weight and it has been proved its durability and reliability by manual flight test. The manual flight test is conducted 10 times for testing its flight performance whether it meets requirement or not. It can fly for 15minutes with 130g payload at around 10 to 15 m/s. The vehicle shows performance that it has a directional stability under crosswind and can be controlled to prevent the MAV entering spin mode. Also, it does not lose the controllability in stall test at a high angle of attack. Although there is leading edge stall, the MAV can be controlled keeping stability because the motor provides inflow continuously to the elevator and rudder. Fig.13 shows flight test of MAV.

Fig.13 Picture of manual flight test

3. Control and Navigation System Design

3.1 System Modeling and Identification

The first step in designing a controller for an aircraft is to characterize its dynamics. There are two approaches for system dynamics identification.

The one approach is aerodynamic based method. This approach can provide nonlinear aerodynamic equations for lumped model. However, it needs extensive modeling and tests on aerodynamic components and often outputs inaccurate results on aerodynamic characteristic. Although there are many aerodynamic analysis tools such as XFLR, DATCOM, and FLUENT and more., they usually generates inaccurate results for small unmanned aerial vehicles (UAVs) due to their very low Reynolds number and highly nonlinear effects such as laminar separation bubbles, quite common to low Reynolds number cases. The other method is a model based parameter identification approach. In this method, a high fidelity model can be obtained with proper data set. On the other hand, the careful experiment design, execution and identification algorithms process are required.

The latter approach is more suitable for modeling MAVs and small UAVs to design linear controllers when the platform is available to test in outdoor and flight data acquisition is relatively easier than using aerodynamic analysis tools.

The target MAV's linear SISO models can be obtained by identification algorithms such as MATLAB Identification Toolbox. Using such tools, one can obtain longitudinal dynamics using elevator servo PWM as input and the pitch angle as output. The others are for lateral dynamics using rudder servo PWM as input and the roll and yaw angle as output respectively [14,15].

The frequency-response method for system identification is widely used to accurately characterize the dynamic response behavior of fixed wing aircraft and rotorcrafts. The recommended input for frequency-domain identification is a frequency sweep because it provides a fairly uniform spectral excitation over the frequency range of interest for good frequency-response identification and is robust to uncertainties in a priori knowledge of the system dynamics. [15, 16]

The flight data-based system identification process uses the input and output of the system and find structured of unstructured model to minimize the error between the recorded and predicted error. [16] The MATLAB's System Identification Toolbox offers a variety of identification tools that can find models with quite good match with the real model.

As can be seen in Fig.14, the test pilot excites sine sweep-like stick commands using radio transmitter during the flight test when the vehicle is in a level steady flight. The following Fig.14 is from the test flight data for obtaining roll, pitch and yaw response models. The flight data is recorded at 20ms internal.

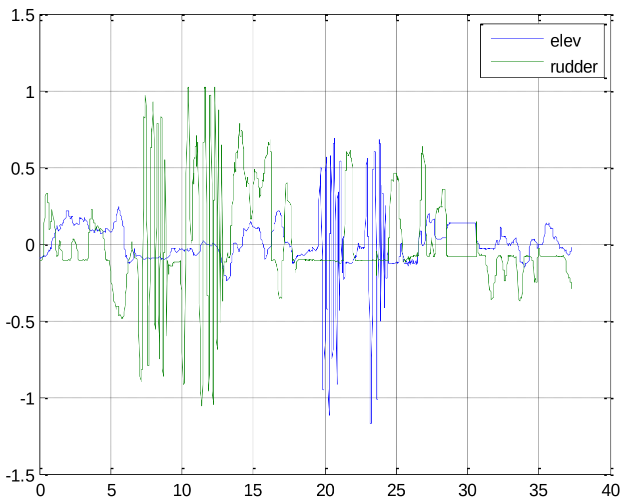

Fig.14 Pilot input commands during ID test flight

The sign convention of control surface deflection angle is used in the model follow a common industry conventions and are given in Table. 7. [17]

Table. 7 Control-Surface Sign Conventions

	Deflection	Sense	Primary Effect
Elev.	Trailing edge down	Positive	(−)Pitching moment
Rudd.	Trailing edge left	Positive	(−)Yawing moment
			(−)Rolling moment

If the small trim angles and small perturbation motion is assumed in system identification maneuvers, the Euler relationships simplify greatly to the linearized equations as follows. [15]

$$\begin{bmatrix} p = \dot{\phi} \\ q = \dot{\theta} \\ r = \dot{\psi} \end{bmatrix} \Rightarrow \begin{bmatrix} p = s\phi \\ q = s\theta \\ r = s\psi \end{bmatrix} \tag{3.1}$$

Using these relationship, the roll, pitch and yaw responses model is estimated. The estimation algorithm is chosen by verification of estimation results whether it has physical meaning or not. The model parameters are found by using ARX and N4SID estimation algorithm. The ARX is a linear difference equation that relates the input to the output. The N4SID estimate state-space models using subspace method [18].

The estimation results are obtained by considering fitting rate and frequency response which is provided by MATLAB. The SISO models are represented by transfer functions in Eqs. (3.2)-(3.4).

For the roll response, the pilot gives the roll command in a sine sweep like manner using rudder, as shown in Fig.15. The vehicle makes positive rolling with negative rudder deflection. The Fig.15 shows that the roll response estimation result.

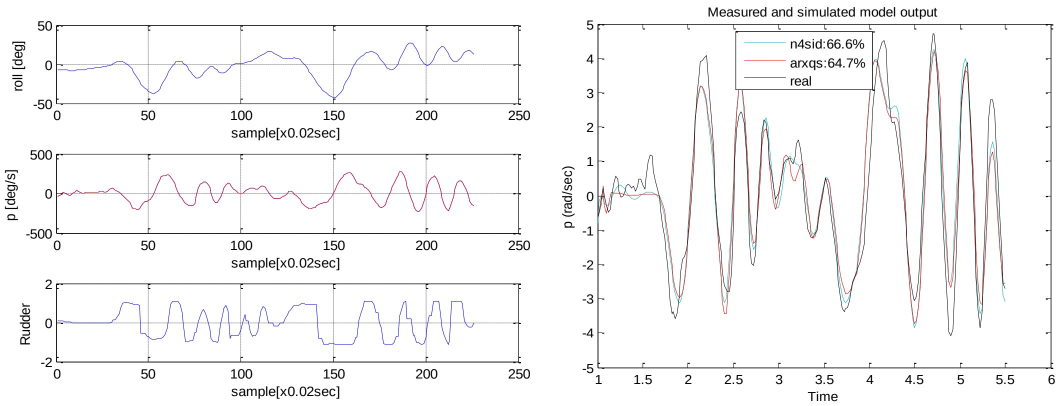

Fig.15 Roll response ID data and estimation result

$$\frac{\phi}{\delta_{rudd}} = -\frac{2.1754(s-111.6)(s^2+33.01s+2298)}{s(s^2+40.41s+500.1)(s^2+9.239s+412.5)} \tag{3.2}$$

For the pitch response, the pilot gives the elevator command as same way in roll model identification using elevator as shown in Fig.16. The Fig.16 and Eq.(3.3) are the pitch response estimation result.

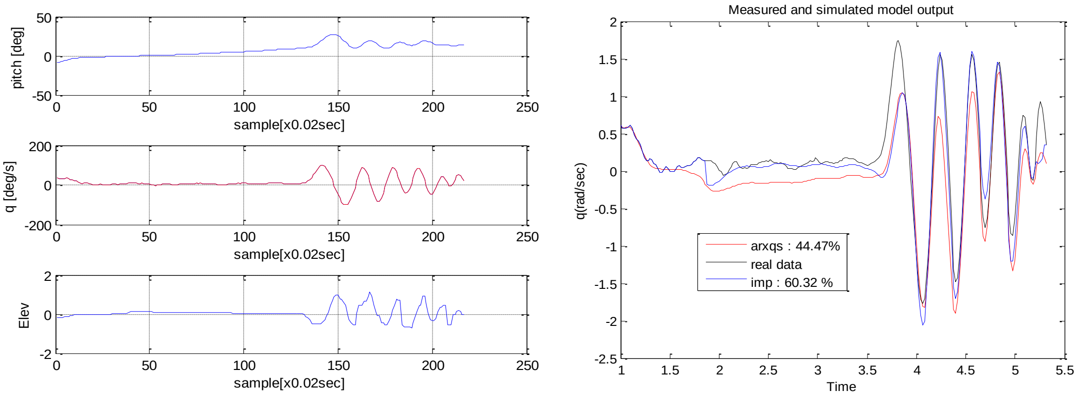

Fig.16 Pitch response ID data and estimation result

$$\frac{\theta}{\delta_{elev}}(s) = -\frac{0.007527(s-186.4)(s+199.1)(s+31.68)(s^2+336.5s+5.407e4)}{s(s+11.74)(s^2+16.36s+495.4)(s^2+233.9s+3.835e4)} \tag{3.3}$$

For the yaw response, the rudder command excites by pilot as shown in Fig.17. The Fig.17 and Eq.(3.4) are the pitch response estimation result.

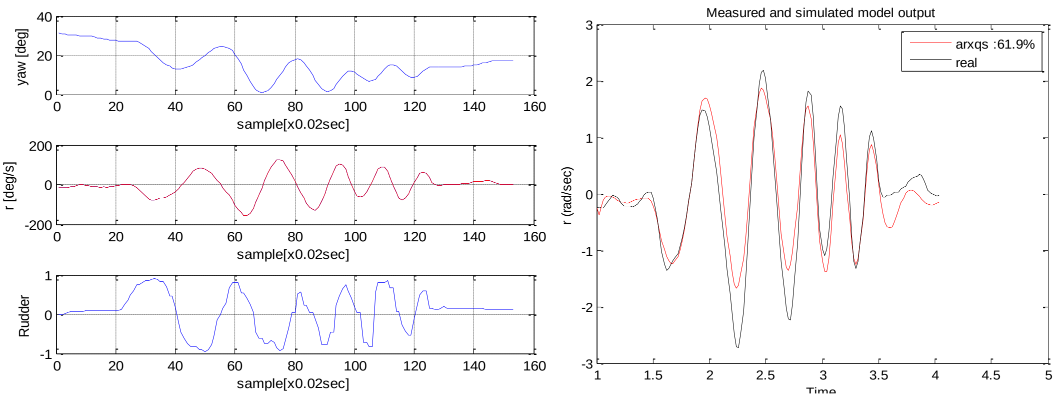

Fig.17 Yaw response ID data and estimation result

$$\frac{\psi}{\delta_{rudd}}(s) = \frac{0.00066982\,(s+193.4)\,(s+10.49)\,(s^2-327.8s+5.572e5)}{s(s+127.5)(s+21.51)(s^2+9.119s+291.3)} \tag{3.4}$$

MAV models are obtained by using estimation algorithms such as N4SID and ARX with MATLAB Identification Toolbox. The SISO models are represented by transfer functions and used to determined gains of attitude controller.

3.2 Controller Design

The autopilot controller is obtained by using the SISO models of MAV. To determine the feedback controller gains, the closed loop step responses are considered with various gains as shown in Figs.18-20. The gains are initially set to 0.7, 0.6 and 0.5 for pitch, roll and yaw respectively. The gains are tuned by a series of flight tests.

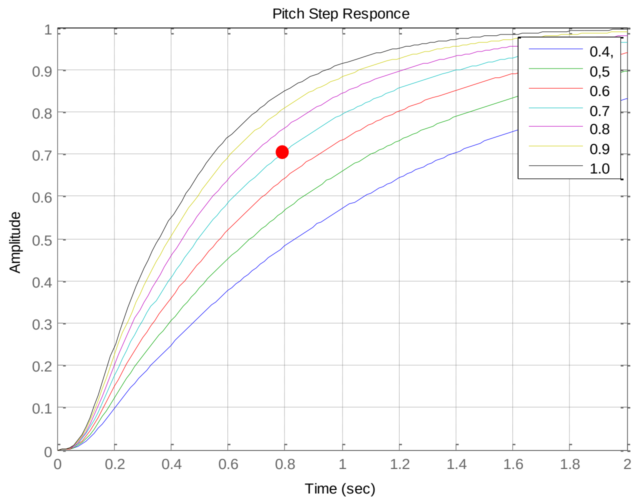

Fig.18 Pitch step response

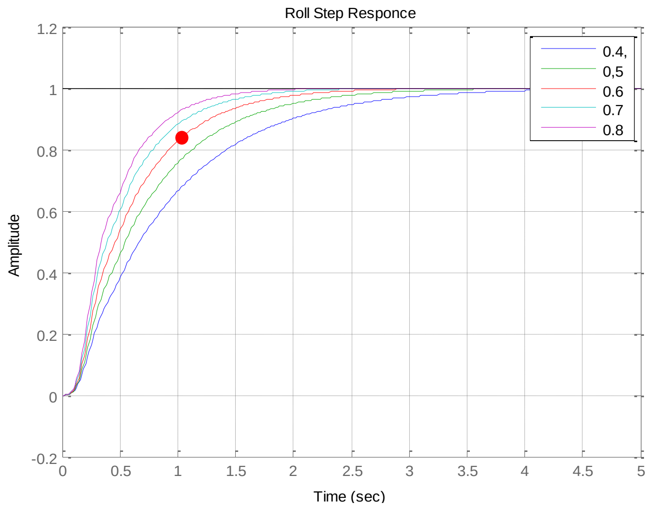

Fig.19 Roll step response

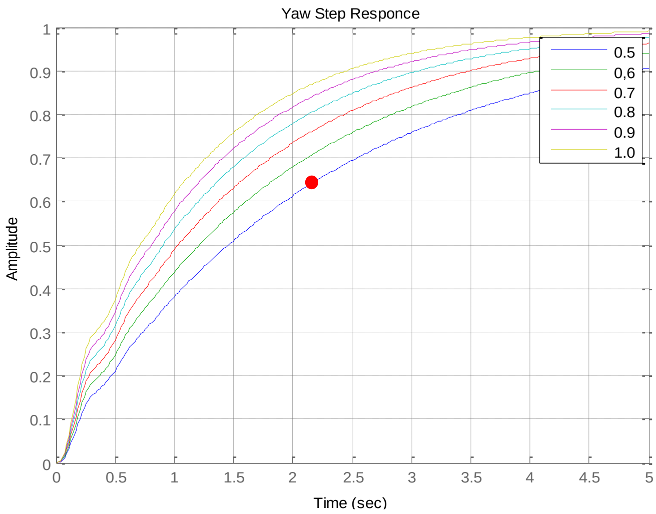

Fig.20 Yaw step response

The controller is designed based on multi-loop PID controller. Since the vehicle has a rudder for rolling, the roll control input actuates rudder servo. The controller provides a roll angle feed-forward term which couples the roll and pitch commands for smooth coordinated turn as shown in Fig.21.

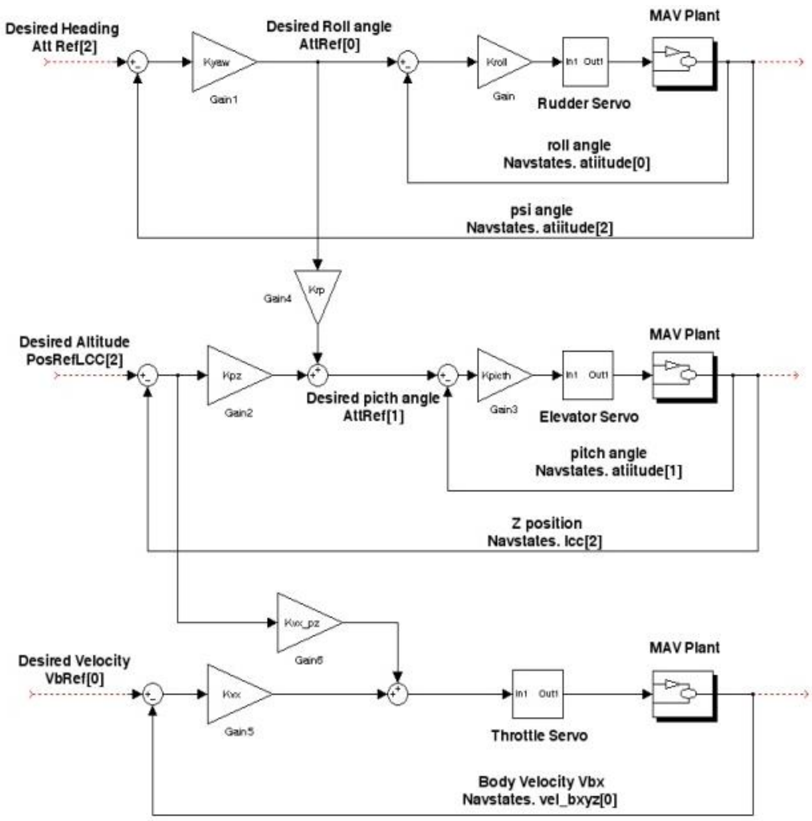

Fig.21 Multi-loop PID controller

The roll and pitch angle limits are set to 50 deg and 20 deg respectively to prevent stall and deep rolling which causes weakening of altitude control performance. The desired heading and altitude can be calculated by the geometric relation between designated waypoints and vehicle navigation position. The speed controller is controlled to track desired velocity and compensate the required thrust to attain desired altitude.

3.3 Navigation System

The inertial navigation system (INS) provides the vehicle motion estimates such as position, velocity and attitude by processing the inertial quantities sensed by inertial measurement unit (IMU). The strap-down INS is suitable for small-size vehicle applications such as MAV due to its size and weight.

The INS alone, however, has error in its integrated solution that grows unbounded as time lapses. Hence, the INS solution must be periodically corrected by external aids. One method is the correction with GPS which provides position and velocity information with bounded error. Therefore, the enhanced navigation system can be achieved to provide highly accurate navigation solutions by loosely coupled GPS/INS integration which has an advantage of simple structure and easy implementation compared with tightly coupled GPS/INS system [18].

The navigation solution is obtained by GPS/INS integration Kalman filter that is feedback method to calibrate the INS information.

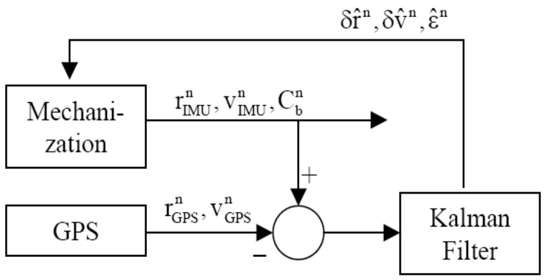

Fig.22 Feedback method of Kalman filter

The position information is used to calibrate the INS data only. The white noise covariance matrix which is called process noise is composed Q matrix that is given by standard deviations of accelerometers and gyroscopes. While the measurement noise R matrix can be obtained from GPS processing, the Q values which are design parameters of filter depend on integration of GPS and IMU sensor performances [18]. Hence, the Q tuning test is necessary to obtain adequate navigation solutions comparing with known position information. After several tests the Q values are determined for best performance.

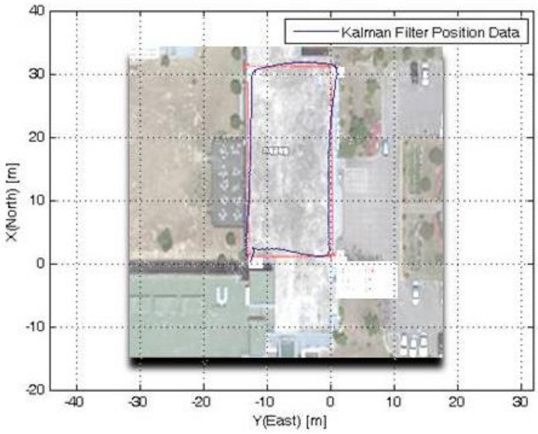

Fig.23 Kalman filter tuning test using known positions

4. AUTOPILOT SYSTEM

The autopilot system is responsible for the overall vehicle management such as vehicle guidance, control and communication. To carry out those sustaining flight of vehicle it should have real-time and high-speed performance. In additions, it should be light and small with all those capability in case of integration for small UAV such as a MAV. To meet these design requirement and restrictions on payload the sensor and flight computer is chosen in consideration of its weight, size and performance. The structure of the flight control system of MAV is shown in Fig.24.

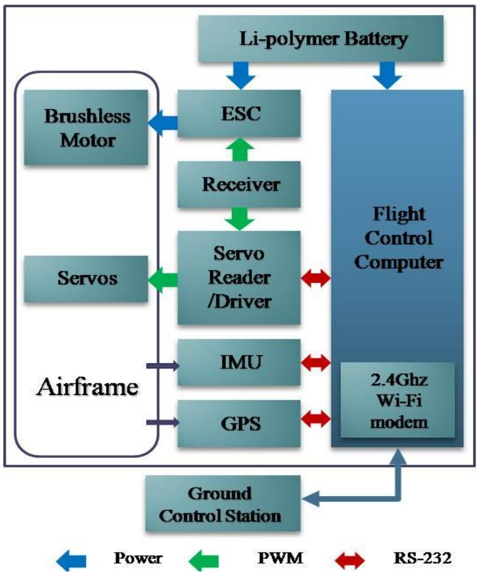

Fig.24 the MAV flight control system configuration

The autopilot system consists of flight control computer, GPS receiver, IMU, and PWM board. The description of these components will be discussed later in more detail.

4.1 Flight Control Computer

The Flight control system consists of a CPU board and expansion boards such as a communication board which includes wireless 802.11b/g, PWM generation board. In this research, the CPU board is built on a PXA 270 400 MHz processor with 64MB RAM and 16MB Flash memory. Since it has only 8g and small size of 80mm x 20mm in spite of its high speed performance, it is the most appropriate computer not only for low level control, but high level control such as a formation flight and so on.

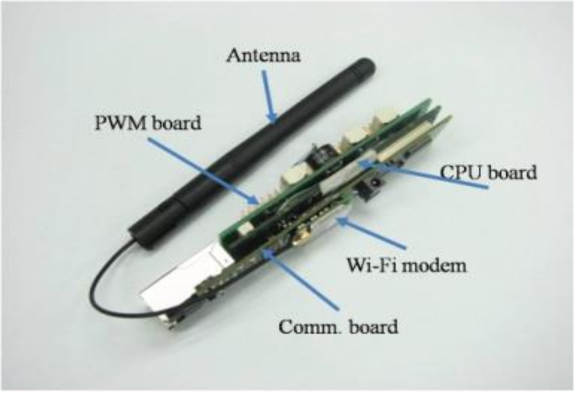

Fig.25 Flight control system

4.2 System Integration

The hardware consists of flight control computer which has an embedded Wi-Fi modem, GPS and IMU. The IMU is chosen in criterion of high performance with light weight and small size. 3DM-GX2 measures accelerations and angular rates as IMU in three axes. The information is used to estimate vehicle state such as position, velocity and attitude in GPS/INS filter.

The U-blox GPS sensor provides three-dimensional positions and time with deduced estimates of velocity and heading. It also has small size and light weight with its high performance. The provided position and velocity data is used as measurement of Kalman filter to calibrate the INS error.

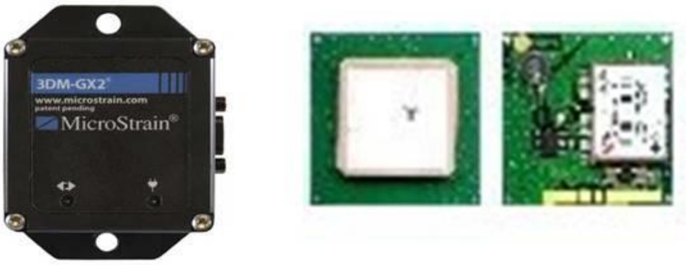

Fig.26 3DM-GX2 (Left) and U-blox GPS(Right)

5. FLIGHT EXPERIMENT

5.1 Attitude Hold SAS Flight test

The flight test is performed to verify the controller for autonomous flight. Before the test flight, the gains are initially set based on pilot's experience at ground. While it shows acceptable flight performance, a series of test flights have been flown. The gain tuning is carried out during its flight. The attitude hold SAS test result is shown in Fig.27. It shows the entire angle history of vehicle and result of attitude hold controller test.

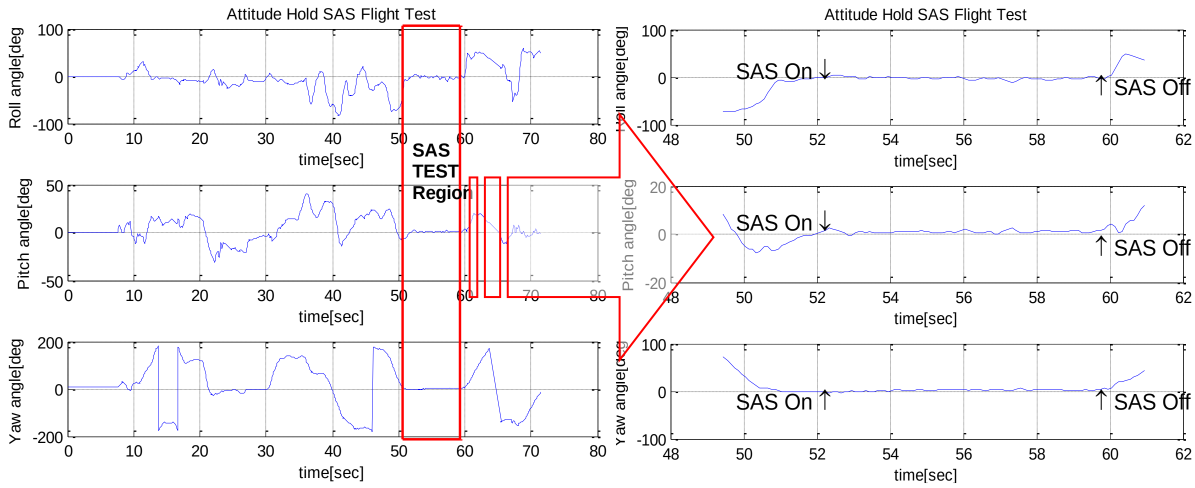

Fig.27 Attitude hold SAS test result

As you can see in Fig.27, the roll and pitch angel goes to about 0 deg and the yaw angle is sustained at initial reference heading angle when the command is on.

5.2 Waypoint Navigation Test

The waypoints are set at (-35, 20,100), (0, 65,100) and (30, 20,100) in local Cartesian coordinate. The waypoint navigation controller checks whether the vehicle reaches the destinations within 10m from each waypoint and commands going next waypoint when it have reached or it does not attain the waypoint in 30 sec.

The flight test is conducted under southwestern wind at 1~2m/s. As you can see in Fig.28 and Fig.29 the vehicle flies clearly around the each desired waypoints. This successful trial validates the design philosophies employed and verified the vehicle performance.

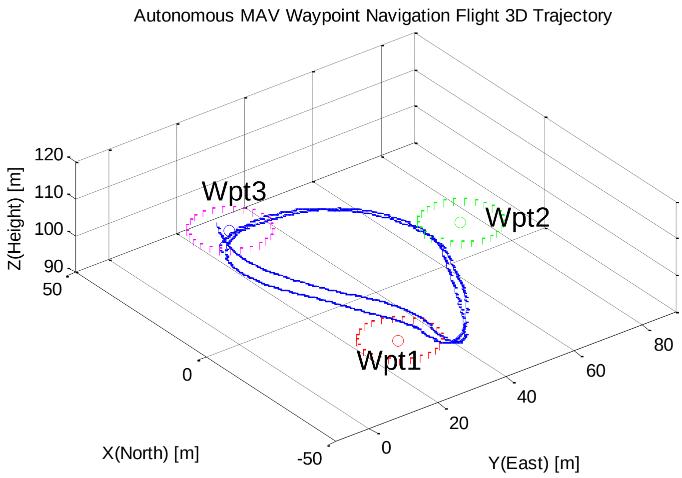

Fig.28 3D waypoint navigation test result

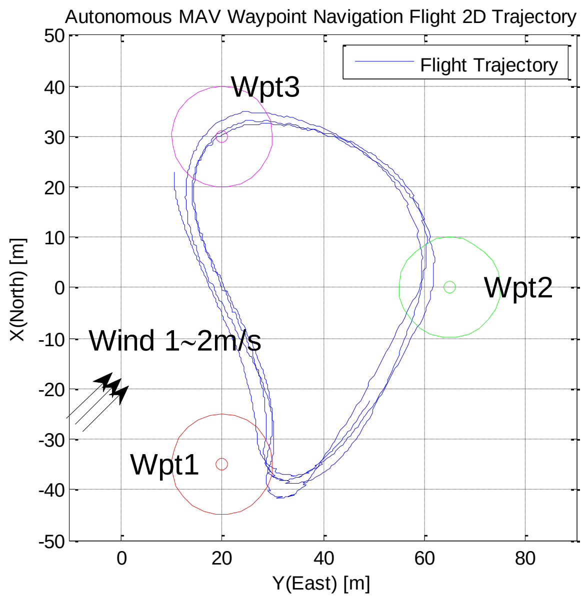

Fig.29 2D waypoint navigation test

Fig.30 KAIST MAV in autonomous flight

6. Autonomous Formation Flight

An autonomous formation flight of UAVs has been vigorously studied for various applications such as search and rescue (SAR) and cooperative missions of multi-agents for task allocation. When the UAVs operate the mission with formation, the UAVs have advantages of strategic mission achievement such as extension of their reconnaissance range and increase offensive power of UAVs.

There are two approaches on formation flight formulation. The first one is the trajectory tracking method which is appropriate for small and larger formation with prescribed maneuvering. The other one is 'leader – follower' formation method which is preferred rather than trajectory tracking because it is appropriate for tracking arbitrary maneuvering of leader vehicle and is has conceptual simplicity in which, the formation flight problem is reduced to a set of tracking problems that can be analyzed and solved using standard control techniques. [19]

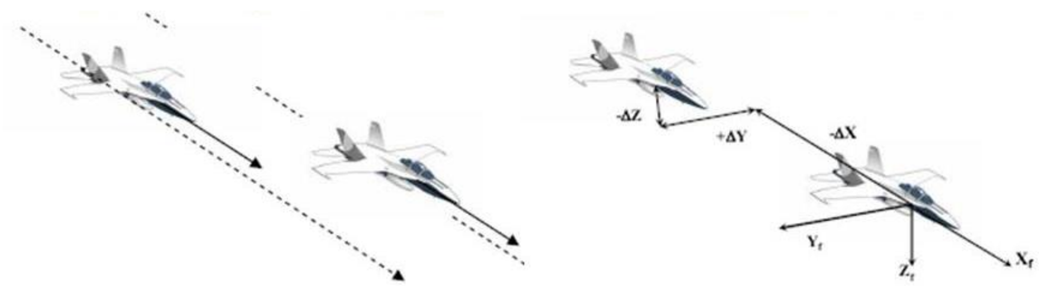

Fig.31 Trajectory Tracking (Left) and 'Leader-Follower' (Right)

To guide and preserve the formation, there are two approaches. The first one is vision or sensor based formation method. These use line of sight (LOS) angle and relative distance between UAVs only. [20] However, in this case, the relative distance may not be estimated accurately due to vision or radar sensor noises, its resolution, low update rate and narrow field or view (FOV). Furthermore, since the performance of formation depends on sensor capability only, it is not adequate approach for a formation flight of small size UAVs which have low payload because the capabilities of small and light cameras and sensors are limited.

The second is formation under inter-communication between UAVs, this method is transferring the each vehicle states to form and keep the formation. In this case, the followers are able to track the leader and maintain the formation under the arbitrary maneuvering of leader which flies autonomously. Moreover, since the most of the UAVs have communication onboard modem, formation flight using inter-communication is easily implemented.

In this research, the latter approach is chosen for formation flight because micro vehicles (MAVs) have a limit on payload. The control law for formation flight is designed via 'leader - follower' formation method with active link using high speed modem to communicate each vehicle states. The main objective of controller design is to maintain the formation geometry under maneuvered flight conditions. The controller is to minimize forward, lateral and vertical error to sustain pre-defined relative clearance.

The designed control law is simulated with PD controller to verify the performance. During the formation flight, it is assumed that there are no communication failures and delay for the simplicity. The virtual and real leader data is used for simulation. The autonomous waypoint navigation flight data of MAV is used as real leader in simulation.

6.1. Problem Formulation

In this section, the relative dynamics are defined to identify formation problem. It assumes that flight path is in a horizontal plane. The position and velocity of vehicles with respect to a local Cartesian coordinate (LCC) are obtained by onboard flight control system which converting filtered GPS/INS position data in longitudinal latitude height (LLH) frame to position in LCC.

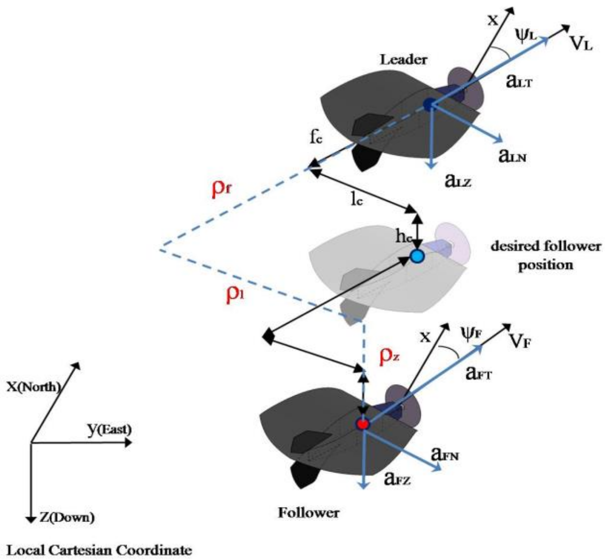

Fig.32 Formation Geometry

As shown in Fig.32, the subscript 'L' and 'F' mean the motion information of leader and follower respectively. The ρ denotes that the relative distance between leader and follower. The ψ is the heading angle of each vehicle with respect to pre-defined local Cartesian coordinate. The V_{xy} means that the projection of the velocity along x and y axis of LCC. The a_{FT}, a_{FN}, a_{FZ} are control inputs u_1, u_2, u_3 for the follower. For the simplicity, it is assumed that the leader and follower are expressed as a point mass model as follows.

$$
\begin{aligned}
\dot{X}_n &= V_{bxy}\cos\psi \\
\dot{Y}_E &= V_{bxy}\sin\psi \\
\dot{Z}_D &= V_{bz} \\
\dot{V} &= a_T,\ \ \dot{\psi} = \frac{a_N}{V}
\end{aligned}
\tag{6.1}
$$

The formation flight control can be decoupled as horizontal and vertical tracking problems [19].

In horizontal geometry, the desired forward clearance f_c and lateral clearance l_c is used as shown in Fig.32. The forward distance ρ_f and lateral distance ρ_l can be expressed as follows.

$$
\begin{gathered}
\rho_x = (x_L - x_F),\quad \rho_y = (y_L - y_F) \\
\begin{bmatrix} \rho_l \\ \rho_f \end{bmatrix} = \begin{bmatrix} \sin\psi_L & -\cos\psi_L \\ \cos\psi_L & \sin\psi_L \end{bmatrix} \begin{bmatrix} \rho_x \\ \rho_y \end{bmatrix}
\end{gathered}
\tag{6.2}
$$

In additions, the derivatives of ρ_f and ρ_l can be derived as follows

$$
\begin{bmatrix} \dot{\rho}_l \\ \dot{\rho}_f \end{bmatrix} = \begin{bmatrix} V_{Fxy}\sin(\psi_F - \psi_L) \\ V_{Lxy} - V_{Fxy}\cos(\psi_F - \psi_L) \end{bmatrix} + \dot{\psi}_L \begin{bmatrix} \rho_f - f_c \\ -\rho_l + l_c \end{bmatrix}
\tag{6.3}
$$

From the Eq.(6.3), the second derivatives of ρ_f and ρ_l can be calculated as

$$
\begin{bmatrix} \ddot{\rho}_l \\ \ddot{\rho}_f \end{bmatrix} = \begin{bmatrix} \dot{V}_{Fxy}\sin(\psi_F - \psi_L) \\ \dot{V}_{Lxy} - \dot{V}_{Fxy}\cos(\psi_F - \psi_L) \end{bmatrix} + \begin{bmatrix} \cos(\psi_F - \psi_L) \\ \sin(\psi_F - \psi_L) \end{bmatrix} V_{Fxy}(\dot{\psi}_F - \dot{\psi}_L) + \begin{bmatrix} \rho_f - f_c \\ -(\rho_l - l_c) \end{bmatrix} \ddot{\psi}_L + \begin{bmatrix} \dot{\rho}_f \\ -\dot{\rho}_l \end{bmatrix} \dot{\psi}_L
\tag{6.4}
$$

It assumes that those vehicles are in a steady wing level or steady sustained turn. Then, the second derivatives of heading angle of leader can be vanished. Taking Eq.(6.1), the Eq.(6.4) is given by

$$
\begin{bmatrix} \ddot{\rho}_l \\ \ddot{\rho}_f \end{bmatrix} = \begin{bmatrix} a_{FT}\sin(\psi_F - \psi_L) \\ a_{LT} - a_{FT}\cos(\psi_F - \psi_L) \end{bmatrix} + \begin{bmatrix} \cos(\psi_F - \psi_L) \\ \sin(\psi_F - \psi_L) \end{bmatrix} V_{Fxy}\left(\frac{a_{FN}}{V_F} - \frac{a_{LN}}{V_L}\right) + \begin{bmatrix} \dot{\rho}_f \\ -\dot{\rho}_l \end{bmatrix} \frac{a_{LN}}{V_L}
\tag{6.5}
$$

6.2 Formation Control Law

It is necessary to find the formation control law using feedback linearization for applying PD controller. The obtained formation dynamics in previous chapter can be expressed in forms of as follows.

$$\begin{bmatrix} \ddot{\rho}_l \\ \ddot{\rho}_f \end{bmatrix} = \begin{bmatrix} \sin(\psi_F - \psi_L) & \cos(\psi_F - \psi_L) \\ -\cos(\psi_F - \psi_L) & \sin(\psi_F - \psi_L) \end{bmatrix} \begin{bmatrix} a_{FT} \\ a_{FN} \end{bmatrix} + \begin{bmatrix} -\frac{V_F}{V_L} + a_{LN}\cos(\psi_F - \psi_L) + \frac{a_{LN}}{V_L}\dot{\rho}_f \\ a_{LT} - \frac{V_F}{V_L} a_{LN}\sin(\psi_F - \psi_L) - \frac{a_{LN}}{V_L}\dot{\rho}_l \end{bmatrix} \tag{6.6}$$

To guide and keep the formation, it is important to define the proper desired output. The output is set as

$$y = [\rho_l \;\; \rho_f]^T, \;\; y_d = [\rho_{l_d} \;\; \rho_{f_d}]^T \tag{6.7}$$
$$where \quad \rho_{l_d} = \rho_l - l_c, \; \rho_{f_d} = \rho_f - f_c$$

From the Eqs.(6.6) and (6.7), it can be rewritten as

$$\begin{bmatrix} \ddot{y}_1 \\ \ddot{y}_2 \end{bmatrix} = \begin{bmatrix} -\frac{V_F}{V_L} + a_{LN}\cos(\psi_F - \psi_L) + \frac{a_{LN}}{V_L}\dot{\rho}_f \\ a_{LT} - \frac{V_F}{V_L} a_{LN}\sin(\psi_F - \psi_L) - \frac{a_{LN}}{V_L}\dot{\rho}_l \end{bmatrix} + \begin{bmatrix} \sin(\psi_F - \psi_L) & \cos(\psi_F - \psi_L) \\ -\cos(\psi_F - \psi_L) & \sin(\psi_F - \psi_L) \end{bmatrix} \begin{bmatrix} u_1 \\ u_2 \end{bmatrix} \tag{6.8}$$

Since the (2 × 2) matrix relating input is invertible, control inputs by using feedback linearization can be derived as follows.

$$\begin{bmatrix} u_1 \\ u_2 \end{bmatrix} = \begin{bmatrix} \sin(\psi_F - \psi_L) & -\cos(\psi_F - \psi_L) \\ \cos(\psi_F - \psi_L) & \sin(\psi_F - \psi_L) \end{bmatrix} \cdot \left(\begin{bmatrix} \ddot{y}_1 \\ \ddot{y}_2 \end{bmatrix} - \begin{bmatrix} -\frac{V_F}{V_L} + a_{LN}\cos(\psi_F - \psi_L) + \frac{a_{LN}}{V_L}\dot{\rho}_f \\ a_{LT} - \frac{V_F}{V_L} a_{LN}\sin(\psi_F - \psi_L) - \frac{a_{LN}}{V_L}\dot{\rho}_l \end{bmatrix} \right) \tag{6.9}$$

From Eq.(6.9), the desired output is defined to cancel the non-linearities.

$$\ddot{y} = \ddot{y}_d, \;\; \ddot{y}_d = \begin{bmatrix} \ddot{\rho}_{l_d} \\ \ddot{\rho}_{f_d} \end{bmatrix} = \begin{bmatrix} -k_{ls}\dot{\rho}_l - k_l(\rho_l - l_c) \\ -k_{fs}\dot{\rho}_f - k_f(\rho_f - f_c) \end{bmatrix} \tag{6.10}$$

Then, there always exists gains to stabilize the above linear system exponentially. Also, it satisfies that ρ_{l_d}, ρ_{f_d} is equal to zero when initial ρ_l and ρ_f are the same as l_c, f_c respectively. In case of that the initial value of ρ_{l_d}, ρ_{f_d} or first derivative of it are not equal to zero, the ρ_{l_d}, ρ_{f_d} go to zero as time lapses [21].

In vertical geometry, the desired vertical clearance h_c is defined as below in Fig.32.

$$\rho_{z_d} = \rho_z - h_c$$
$$where \quad \rho_z = h_L - h_F \tag{6.11}$$

Then, control input u_3 can be obtained by same as in horizontal.

$$\begin{aligned}\dot{\rho}_{z_d} &= \dot{\rho}_z \\ &= V_{LH} - V_{FH} \\ \ddot{\rho}_{z_d} &= \ddot{\rho}_z \\ &= a_{LZ} - a_{FZ} = a_{LZ} - u_3 \\ u_3 &= a_{LZ} - \ddot{\rho}_{z_d}\end{aligned} \tag{6.12}$$

Then, ρ_{Z_d} is defined as below and control input u_3 is in Eq.(6.13)

$$\begin{aligned}\ddot{\rho}_{z_d} &= -k_{zs}\dot{\rho}_z - k_z(\rho_z - h_c) \\ u_3 &= a_{LZ} + k_{zs}\dot{\rho}_z + k_z(\rho_z - h_c)\end{aligned} \tag{6.13}$$

Since these control law is derived based on communication of vehicle states the communication delay have to be considered for implementation of this controller later.

6.3 Simulation Results

Simulation is performed to verify the derived control law. The assumption is that the leader transmits its states to follower vehicle such as LCC position, velocity, Euler angles and acceleration which are sampled from leader IMU with 16 Hz. The performance of two vehicles is assumed as same.

The first simulation condition is presented in Table. 1. The virtual leader is commanded as it seems to fly for autonomous waypoint navigation during the simulation. The virtual leader input is set with normal acceleration only. The follower acceleration is bounded as follows.

$$\left| \begin{bmatrix} a_{FT} & a_{FN} & a_{FZ} \end{bmatrix}^T \right| \le \begin{bmatrix} 2 & 15 & 3 \end{bmatrix}^T \; (m/s^2)$$

Table. 8 Initial conditions of first simulation

Conditions	Leader	Follower
Position (m) (x,y,z)	0, 0, 100	-20, -20, 80
Heading(deg)	30	-30
V_{init} in xy plane	15	16
V_{init} in z plane	0	0

The forward, lateral and height clearance are set as follows.

$l_c = 10m,\ f_c = 10m,\ h_c = 10m$

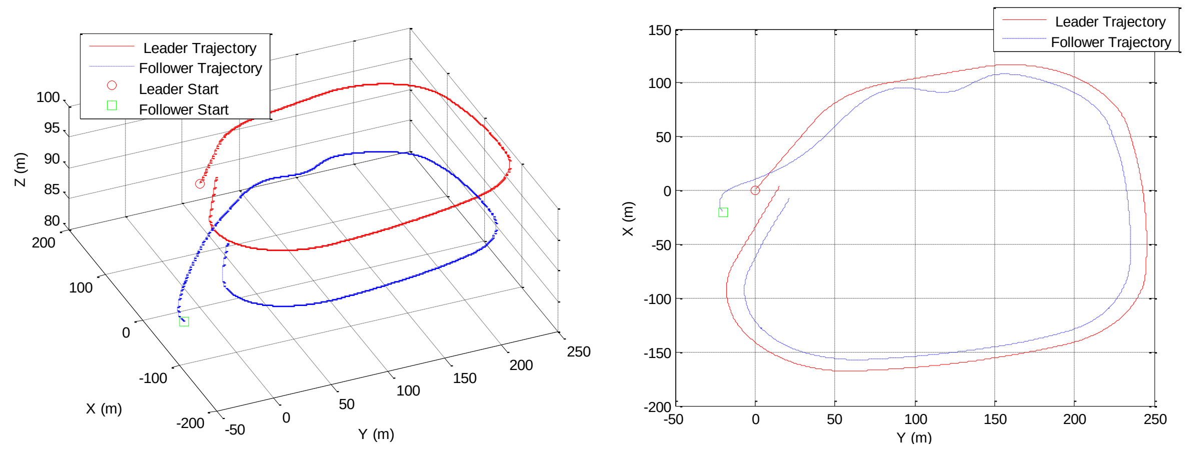

Fig.33 Formation flight trajectory (3D-Left, 2D-Right)

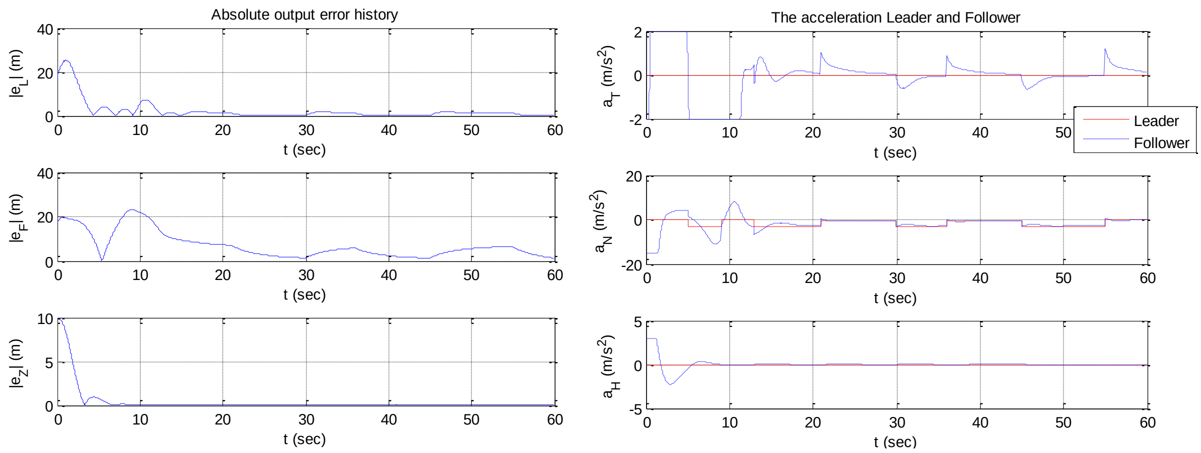

Fig.34 Formation error (Left) and Control input history (Right)

The first simulation result shows that the follower can track the virtual leader under smooth roll maneuver after about 30 seconds for approaching formation.

The second simulation is performed using real leader flight data. The MAV's autonomous waypoint navigation flight data is used.

Table. 9 Initial conditions of first simulation

Conditions	Leader	Follower
Position (m) (x,y,z)	27.8, -2.04, 104.6	47.8,-12.04, 84.6
Heading(deg)	-172	-172
V_{init} in xy plane	10.6	13.0

V_{init} in z plane	-0.3	0

The forward, lateral and height clearance are set as same with first simulation.

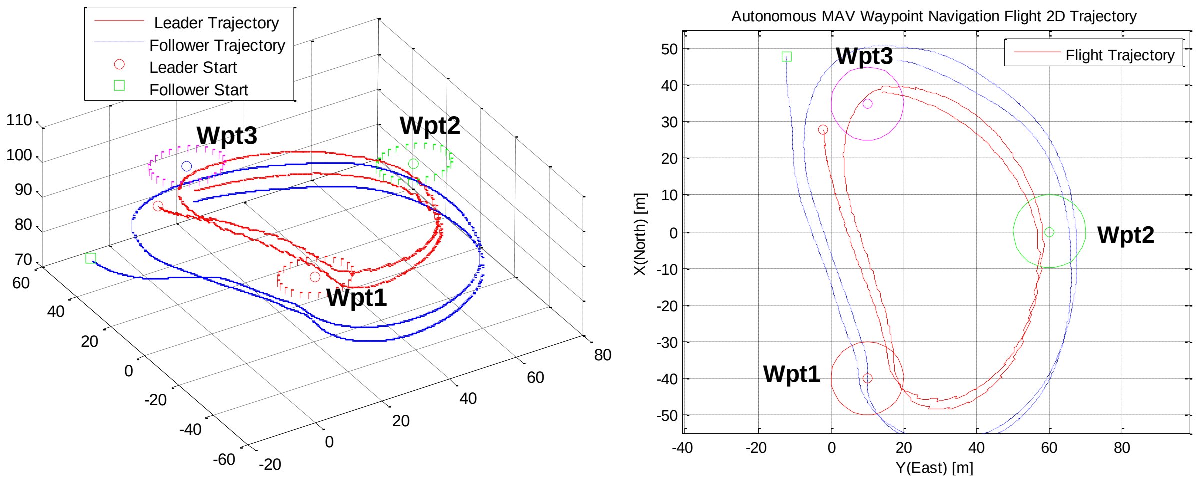

Fig.35 Formation flight trajectory (3D-Left, 2D-Right)

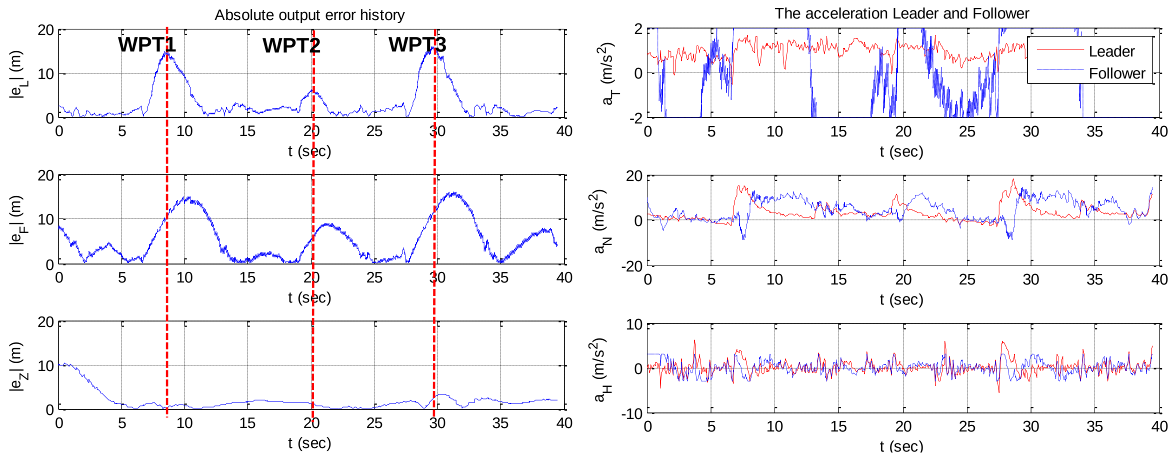

Fig.36 Formation error (Left) and Control input history (Right)

As can be seen in Figs.35-36, the follower is able to maintain the formation with the leader except around each waypoint. When the leader reaches the waypoints, it is commanded to go to next waypoint with a large normal acceleration. The tracking errors are generated because of the assumptions that the leader is in level flight and coordinate turn condition. Although the formation errors increase near waypoints for reasons of this, the follower shows a good performance between waypoints during the simulation. As can be seen with 2nd simulations, the nonlinear formation control law is needed for more accurate and tight formation.

7. Conclusions

A mission profile for the MAV is proposed for requirement of vehicle and autopilot. The aircraft design is carried out the conventional design procedures. THT is applied to analyze and develop vehicle airfoil. An In-house CATIA – MATLAB code is developed for analysis. The propulsion system is chosen by using thrust calculator with various motors, propellers and batteries. It satisfies the design requirements such as maximum size, weight and payload.

Then, the high speed flight computer is developed to operate multi-flight processes such as navigation, GPS, communications and so on. A micro autopilot is developed for an autonomous MAV which has a low payload. It is designed by using 400 MHz CPU with 64MB RAM and 16MB flash memory. This makes it possible to apply high level control such as multi-MAVs formation flight and other modern controllers like L1 adaptive control and so on. The autopilot is integrated by combinations of GPS, IMU, flight computer and PWM board. A loosely coupled GPS/INS filter is implemented to estimate accurate vehicle navigation information and to ensure operational reliability.

MAV models are obtained by using estimation algorithms such as N4SID and ARX with MATLAB Identification Toolbox. The SISO models are represented by transfer functions and used to determine gains of attitude controller. For the autonomous navigation flight, the multi-loop PID controller is designed. The controller consists of attitude, altitude and speed controller. With the reference heading angle guidance loop, the MAV performs waypoint navigation flight autonomously. The autonomous waypoint flight result shows a good performance of the proposed MAV system and is turned out to be robust under cross wind environment. It can reach the destinations within 10m from waypoint. For the more accurate navigation and robustness of flight performance under wind disturbances it is necessary to employ the trajectory tracking controller and integral gains of PID controller.

Finally, the autonomous formation flight control law is proposed and verified. It is designed via ‘leader-follower’ formation method under inter-communication environment. This control law can be easily extended to apply to numbers of MAVs. The simulation results show that the follower can track the virtual and real leader.

REFERENCES

[1] US Department of Defense, *Unmanned Systems Roadmap 2007-2032*

[2] R. Krashanitsa, G. Platanitis, B. Silin, S. Shkarayev,“Aerodynamics and Controls Design for Autonomous Micro Air Vehicles,” *AIAA Atmospheric Flight Mechanics Conference and Exhibit*, August 2006, Keystone, Colorado

[3] D. P. Raymer, *Aircraft Design: A Conceptual Approach*, 3rd Edition, *American Institute of Aeronautics and Astronautics*, Inc., Washington. D.C.

[4] D.K. Chung, J.H. Ryu, I.C. Nam, “Development of Fixed Wing MAV ‘Batwing’ at Kunkuk University,” 9th International Micro Air Vehicle Competition, 2005, Kunkuk University, Seoul, South Korea.

[5] H.P. Horton, “Laminar Separation Bubbles in Two and Three-Dimensional Incompressible Flow,” Ph.D. Thesis. University of London, UK. 1968

[6] S. Yarusevych, P. E. Sullivan, J. G. Kawall, “Airfoil Boundary Layer and Wake Development at Low Reynolds Numbers,” *35th AIAA Fluid Dynamics Conference and Exhibit*, Toronto, Ontario, June 6-9, 2005.

[7] K. Nickel, M. Wohlfahrt, “Tailless aircraft in theory and practice,” *American Institute of Aeronautics and Astronautics*, London, England E. Arnold, 1994

[8] University of Florida, “University of Florida Competition Micro Air Vehicle,” 6th International Micro Air Vehicle Competition, Edited by J. Bowman, Brigham Young University, Provo, Utah, Apr. 2002, pp 19-29.

[9] J. D. Anderson, *Fundamentals of Aerodynamics*, McGraw-Hill, Inc., 3rd edition, 2001.

[10] T. J. Mueller, G. E. Torres,"Aerodynamics Characteristics of Low Aspect Ratio Wings at Low Reynolds Numbers," *Fixed and Flapping wing Aerodynamics for Micro Air Vehicle Applications*. Progress in Astronautics and Aeronautics, 2001

[11] RCLAB, model aircraft design (http://www.rclab.co.kr)

[12] Y.B. Lee, U.R. Kim, K.H. Kim, J.A. Kim, “Development of SNU Micro Aerial Vehicle via Experimental study,” *the Korean Society for Aeronautical and Space Sciences* , Vol.34, No.11, 2006

[13] Drive Calculator(http://www.drivecalc.de/)

[14] J. Nino, F. Mitrache, P. Cosyn, R. D. Keyser, “Model Identification of a Micro Aerial Vehicle,” *Journal of Bionic Engineering*, pp227-236, 2007.

[15] M.B. Tischler, R.K. Remple, *Aircraft and Rotorcraft System Identification Engineering Methods with Flight Test Examples*, American Institute of Aeronautics and Astronautics, Inc., Reston, Virginia.

[16] H.C. Shim, “Hierarchical Flight Control System Synthesis for Rotorcraft-based Unmanned Aerial Vehicles,” Ph.D Thesis, University of Berkeley, December, 2000.
[17] B. L. Stevens, *Aircraft control and Simulation 2nd edition*, 1992, John Wiley& Son, inc
Mathworks Inc. MATLAB 2007a, (http://www.mathworks.com/products/sysid)
[18] E.H. Shin, “Accuracy Improvement of Low Cost INS/GPS for Land Applications,” MS. Thesis, University of Calgary, December, 2001.
[19] Y. Gu. B. Seanor, G. Campa, M.R. Napolitano, L. Rowe, S. Gururajan, W. Sheng, “Design and Flight Testing Evaluation of Formation Control Law,” *IEEE Transactions on Control System Technology*, Vol.14, No.6, November 2006
[20] C.K Ryoo, Y.H. Kim, M.J. Tahk, “Optimal UAV formation guidance laws with timing constraint,” *International Journal of Systems Science*, Vol.37, 2006
[21] H.K. Khalil, *Nonlinear System*, Prentice hall inc. New Jersey, 3rd edition, 2002.